AVATARGO: ZERO-SHOT 4D HUMAN-OBJECT INTERACTION GENERATION AND ANIMATION

Anonymous authors
Paper under double-blind review

ABSTRACT

Recent advancements in diffusion models have led to significant improvements in the generation and animation of 4D full-body human-object interactions (HOI). Nevertheless, existing methods primarily focus on SMPL-based motion generation, which is limited by the scarcity of realistic large-scale interaction data. This constraint affects their ability to create everyday HOI scenes. This paper addresses this challenge using a zero-shot approach with a pre-trained diffusion model. Despite this potential, achieving our goals is difficult due to the diffusion model's lack of understanding of *"where"* and *"how"* objects interact with the human body. To tackle these issues, we introduce **AvatarGO**, a novel framework designed to generate animatable 4D HOI scenes directly from textual inputs. Specifically, **1)** for the *"where"* challenge, we propose **LLM-guided contact retargeting**, which employs Lang-SAM to identify the contact body part from text prompts, ensuring precise representation of human-object spatial relations. **2)** For the *"how"* challenge, we introduce **correspondence-aware motion optimization** that constructs motion fields for both human and object models using the linear blend skinning function from SMPL-X. Our framework not only generates coherent compositional motions, but also exhibits greater robustness in handling penetration issues. Extensive experiments with existing methods validate AvatarGO's superior generation and animation capabilities on a variety of human-object pairs and diverse poses. As the first attempt to synthesize 4D avatars with object interactions, we hope AvatarGO could open new doors for human-centric 4D content creation.

1 INTRODUCTION

The creation of 4D human-object interaction (HOI) holds immense significance across a wide range of industries, including augmented/virtual reality (AR/VR) and game development, as it forms the foundation of the 4D virtual world. Traditionally, developing such models has required extensive human effort and specialized engineering expertise. Fortunately, thanks to the collections of HOI datasets (Li et al., 2023b; Bhatnagar et al., 2022; Jiang et al., 2023a) and the recent advancements in diffusion models (Saharia et al., 2022; Ramesh et al., 2022; Balaji et al., 2022; Stability.AI, 2022; 2023), existing HOI generative techniques (Zhang et al., 2022; 2023; 2024; Shafir et al., 2023; Kapon et al., 2024; Chen et al., 2024a) have exhibited promising capabilities by generating 4D human motions with object interactions from textual inputs. Nonetheless, these methods primarily focus on SMPL-based (Loper et al., 2015; Pavlakos et al., 2019) motion generation, which struggles to capture the realistic appearance of subjects encountered in everyday life. Although InterDreamer (Xu et al., 2024b) has recently proposed to generate text-aligned 4D HOI sequences in a zero-shot manner, their output is still largely constrained by the SMPL model. This highlights a pressing need for more realistic and generalizable methods tailored specifically to model 4D human-object interactive content. We take the initiative and showcase the potential of addressing this challenge by leveraging the 3D generative methods in a zero-shot manner.

In recent times, 3D generative methods (Poole et al., 2022; Tang et al., 2023; Liu et al., 2023c; Lin et al., 2023; Wang et al., 2023d; Cao et al., 2023b; Liao et al., 2023) and Large Language Models (LLMs) (Wu et al., 2023a) have garnered increasing interest. These progressives have led to the development of text-guided 3D compositional generation techniques that are capable of comprehending intricate relations and creating complex 3D scenes incorporating multiple subjects. Notably, GraphDreamer (Gao et al., 2023) utilizes LLMs to construct a graph where nodes represent

Figure 1: **Examples of 4D animation results obtained via AvatarGO.** AvatarGO effectively produces diverse human-object compositions with correct spatial correlations and contact areas. It achieves joint animation of humans and objects while avoiding penetration issues.

objects and edges denote their relations. ComboVerse (Chen et al., 2024b) proposes spatial-aware score distillation sampling to amplify the spatial correlation. Subsequent studies (Epstein et al., 2024; Zhou et al., 2024) further explore the potential of jointly optimizing layouts to composite different components.

Despite the promising performance demonstrated by existing methods, they encounter two major challenges in generating 4D HOI scenes: *1) Incorrect contact area:* While LLMs excel at capturing the relationships, optimization with diffusion models faces difficulties in accurately defining the contact area between various objects, particularly those with complex articulated structures like human bodies. Although efforts like InterFusion (Dai et al., 2024) have constructed 2D human-object interaction datasets to retrieve human poses from text prompts, they still encounter challenges in defining the optimal contact body parts for cases outside the training distribution. *2) Limitations in 4D compositional animation:* While existing techniques like DreamGaussian4D (Ren et al., 2023) and TC4D (Bahmani et al., 2024) employ video diffusion models (Blattmann et al., 2023; Guo et al., 2023a) to animate 3D static scenes, they often treat the entire scene as one subject during optimization, leading to unrealistic animation results. Despite initiatives like Comp4D (Xu et al., 2024a), which utilize trajectories to animate 3D objects individually, modeling contact between various subjects remains a challenge.

In this paper, we propose **AvatarGO**, a novel framework for compositional 4D avatar generation with object interactions. By taking the text prompts as inputs, we assume that the 3D human and object models as well as the human motion sequences can be individually generated by adopting existing generative techniques (Tang et al., 2023; Liu et al., 2023d; Zhang et al., 2023; 2024). Specifically, we adopt DreamGaussian4D (Ren et al., 2023) as our baseline considering its superior training efficiency and focus on addressing the challenges associated with human-object interactions. To achieve this objective, AvatarGO integrates two key innovations to learn *"where"* and *"how"* the object should

interact with the human body: **1) LLM-guided contact retargeting.** Given the limited availability of human-object interaction images in the 2D dataset used for diffusion model training, it's difficult to identify the most appropriate contact area between humans and objects. To tackle this issue, we propose leveraging Lang-SAM (lan, 2023) to identify the contact body part from text prompts, which serves as the initialization for the optimization procedure. **2) Correspondence-aware motion optimization.** Building upon the observation that penetration is absent in static composited models, we introduce correspondence-aware motion optimization that leverages SMPL-X as an intermediary to maintain the correspondence between humans and objects when they are animated to a new pose, thus demonstrating greater robustness in handling penetration issues.

We thoroughly assess AvatarGO by compositing diverse pairs of 3D humans and objects and animating them across various motion sequences (see Fig. 1). Our experimental results show that our method excels at identifying optimal contact areas and exhibits greater robustness in handling penetration issues during animation, significantly outperforming existing techniques. We will make our code publicly available.

2 Related Work

3D Content Generation. Leveraging advances in diffusion-based text-to-2D image generation (Saharia et al., 2022; Ramesh et al., 2022; Balaji et al., 2022; Stability.AI, 2022; 2023), DreamFusion introduced Score Distillation Sampling (SDS) to generate 3D content via pre-trained models, utilizing technologies like NeRF (Mildenhall et al., 2020), DMTet (Shen et al., 2021), 3D Gaussian Splatting (Kerbl et al., 2023)). Subsequent research has focused on enhancing output quality (Lin et al., 2023; Chen et al., 2023b; Wang et al., 2023d), controlling generation processes (Metzer et al., 2022; Seo et al., 2023), improving training efficiency (Wang et al., 2023a; Wu et al., 2024; Tang et al., 2023), and extending capabilities on 3D texturing (Richardson et al., 2023; Cao et al., 2023a; Chen et al., 2023a; Tang et al., 2024b). Addressing 3D human body complexity, recent studies (Cao et al., 2023b;c; Liao et al., 2023; Jiang et al., 2023b; Huang et al., 2023b; Kolotouros et al., 2023; Zeng et al., 2023; Huang et al., 2023a) have been proposed for creating controllable 3D human avatars, although these still require significant input-specific training time. The proliferation of large 3D datasets (Deitke et al., 2023; 2024; Wu et al., 2023b) has propelled 3D generation techniques forward. Notably, Zero-1-to-3 (Liu et al., 2023c), Zero123++ (Shi et al., 2023a), and MVDream (Shi et al., 2023b) use 2D diffusion models to generate consistent multi-view images, serving as inputs for efficient 3D model generation tools like SyncDreamer (Liu et al., 2023e), Wonder3D (Long et al., 2023), One-2-3-45 (Liu et al., 2023b;a), UniDream (Liu et al., 2023f), MVDiffusion++ (Tang et al., 2024c), and Make-Your-3D (Liu et al., 2024). Additionally, building on transformer (Vaswani et al., 2017) and image processor advancements (e.g., DINO (Caron et al., 2021; Oquab et al., 2023)), Large Reconstruction Models (Hong et al., 2023; Wang et al., 2023b; Xu et al., 2023; Li et al., 2023a) implement transformer-based architectures to derive 3D tri-plane tokens from image features. 3DTopia (Hong et al., 2024) uses hybrid diffusion priors to produce high-fidelity 3D objects. Meanwhile, methods like LGM (Tang et al., 2024a), CRM (Wang et al., 2024), and GRM (Yinghao et al., 2024) explore various 3D representations for improved performance, such as 3D Gaussian Splatting (Kerbl et al., 2023) and FlexiCube (Shen et al., 2023). Despite these advances, challenges remain in generating complex compositional 3D scenes.

3D Compositional Generation. To address the compositional nature of 3D content, a few efforts have been made recently. *Epstein et al* (Epstein et al., 2024) and GALA3D (Zhou et al., 2024) propose optimizing component layouts for integrated object scenes. ComboVerse (Chen et al., 2024b) introduces spatial-aware score distillation sampling (SSDS) to effectively learn object spatial relations. GraphDreamer (Gao et al., 2023) uses large language models to form graph structures where nodes and edges represent objects and their relationships, respectively, showing promising results. Challenges remain in modeling interactions between humans and objects. InterFusion (Dai et al., 2024) develops a 2D dataset for human-object interactions, enabling text-guided pose retrieval and scene generation. However, this approach lacks precise control over interaction areas and is not readily adaptable to 4D scenarios.

4D Content Generation. Recent advances in video diffusion models and score distillation sampling have spurred a variety of 4D scene generation techniques. Make-A-Video3D (MAV3D) (Singer et al., 2023) utilizes HexPlane features for 4D representations. 4D-fy (Bahmani et al., 2023) and

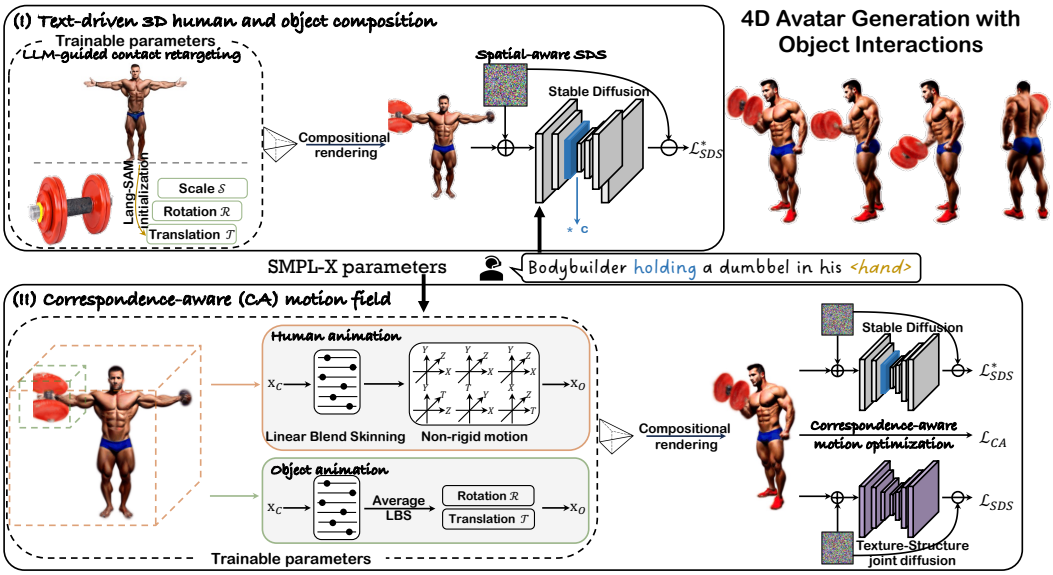

Figure 2: **Overview of AvatarGO.** AvatarGO takes the text prompts as input to generate 4D avatars with object interactions. At the core of our network are: 1) *Text-driven 3D human and object composition* that employs large language models to retarget the contact areas from texts and spatial-aware SDS to composite the 3D models. 2) *Correspondence-aware motion optimization* which jointly optimizes the animation for humans and objects. It effectively maintains the spatial correspondence during animation, addressing the penetration issues.

DreamGaussian4D (Ren et al., 2023) employ multi-stage optimization pipelines to transform static 3D into dynamic 4D scenes. Dream-in-4D (Zheng et al., 2023) allows for personalized 4D generation using image guidance, while Consistent4D (Jiang et al., 2023c) uses video inputs with RIFE (Huang et al., 2022) and a super-resolution module for scene creation. 4DGen (Yin et al., 2023) and AnimatableDreamer (Wang et al., 2023c) focus on controllable motion generation via driving videos. More recently, Comp4D (Xu et al., 2024a) and TC4D (Bahmani et al., 2024) have introduced trajectory-based approaches for creating 4D compositional scenes. While these technologies show promise, they often struggle to produce 4D avatars that effectively interact with objects. Although GAvatar (Yuan et al., 2023) excels in 4D human animation, its object interaction capabilities are limited.

3 Methodology

Given a generated 3D avatar and a specific 3D object, AvatarGO generates compositional 4D avatars with object interactions based on text instructions. In the subsequent sections, we first introduce the preliminaries (in Sec. 3.1), including static 3D content generation and parametric human model SMPL-X. Next, we will describe the key components of AvatarGO, including (1) text-driven 3D human and object composition (in Sec. 3.2), and (2) correspondence-aware motion optimization for achieving synchronized human and object animation (in Sec. 3.3). The overview of AvatarGO is shown in Fig. 2.

3.1 Preliminaries

3D Model Generation. Recently, DreamGaussian (Tang et al., 2023) showcases promising results with largely improved training efficiency by incorporating two major components:

(1) *3D Gaussian Splatting (3DGS).* 3DGS (Kerbl et al., 2023) directly defines the 3D space through a set of Gaussians parameterized by their 3D position μ, opacity α, anisotropic covariance Σ, and spherical harmonic coefficients sh. The sh term is used to capture the view-dependent appearance of

the scene and Σ can be decomposed to:

$$\Sigma = RSS^T R^T, \tag{1}$$

where R is the rotation matrix expressed by a quaternion $q \in \mathbf{SO}(3)$, and S is the scaling matrix, represented by a 3D vector s. Essentially, each Gaussian centered at point (mean) μ is defined as:

$$G(\mathbf{x}, \mu) = e^{-\frac{1}{2}(\mathbf{x}-\mu)^T \Sigma^{-1}(\mathbf{x}-\mu)}, \tag{2}$$

where $\mathbf{x}$ is the 3D query point.

For rendering the 3D Gaussians onto the 2D image space, 3DGS incorporates a tile-based rasterizer and point-based α-blend rendering. Specifically, the color $C(u)$ of a pixel u can be calculated as:

$$C(u) = \sum_{i \in N} T_i c_i \alpha_i \mathcal{SH}(sh_i, v), \quad T_i = G(\mathbf{x}, \mu_i) \prod_{j=1}^{i-1} \left(1 - \alpha_j G(\mathbf{x}, \mu_j)\right), \tag{3}$$

where T represents the transmittance, $\mathcal{SH}$ denotes the spherical harmonic function, and v indicates the viewing direction. By optimizing the Gaussian attributes $\{G : \mu, q, s, \sigma, c\}$ and dynamically adjusting the density of 3D Gaussians (*i.e.*, densifying and pruning), DreamGaussian achieves high-quality generations from either textual or visual inputs.

(2) *Score Distillation Sampling (SDS).* Starting with the latent feature $\boldsymbol{z}$ extracted from a 3DGS rendering $\boldsymbol{x}$, SDS introduces random noise ϵ to $\boldsymbol{z}$, yielding a noisy latent variable $\boldsymbol{z}_t$. This variable is then processed by a pre-trained denoising function $\epsilon_\phi\left(\boldsymbol{z}_t; y, t\right)$ to estimate the added noise. The SDS loss then calculates the difference between predicted and added noise, with its gradient calculated by:

$$\nabla_\theta \mathcal{L}_{\text{SDS}}(\phi, g(\theta)) = \mathbb{E}_{t, \epsilon \sim \mathcal{N}(0,1)} \left[w(t) \left(\epsilon_\phi\left(\boldsymbol{z}_t; y, t\right) - \epsilon\right) \frac{\partial \boldsymbol{z}}{\partial \boldsymbol{x}} \frac{\partial \boldsymbol{x}}{\partial \theta} \right], \tag{4}$$

where y denotes the text embedding, $w(t)$ weights the loss from noise level t. We do not apply the mesh extraction and texture optimization proposed in DreamGaussian to obtain the 3D models.

SMPL-X (Loper et al., 2015; Pavlakos et al., 2019). With pose parameter θ, shape parameter β, and expression parameter ϕ as inputs, SMPL-X maps the canonical model to the observation space:

$$M(\beta, \theta, \phi) = \texttt{LBS}(\boldsymbol{T}(\beta, \theta, \phi), J(\beta), \theta, \mathcal{W}), \tag{5a}$$

$$\boldsymbol{T}(\beta, \theta, \phi) = \mathbf{T} + B_s(\beta) + B_e(\phi) + B_p(\theta), \tag{5b}$$

where M denotes the function defining the mesh model of a human body, and $\boldsymbol{T}$ represents the transformed vertices. $\mathcal{W}$ stands for blend weights, B_s, B_e, and B_p are functions respectively for shape, expression, and pose blend shapes. $\texttt{LBS}(\cdot)$ indicates the linear blend skinning function that poses each body vertex of SMPL-X according to:

$$\mathbf{v}_o = \mathcal{G} \cdot \mathbf{v}_c, \quad \mathcal{G} = \sum_{k=1}^{K} w_k \mathcal{G}_k(\theta, j_k), \tag{6}$$

where $\mathbf{v}_c$ and $\mathbf{v}_o$ represent SMPL-X vertices under the canonical pose and observation space, respectively. w_k is the skinning weight, $\mathcal{G}_k(\theta, j_k)$ is the affine deformation that maps the k-th joint j_k from the canonical space to observation space, and K denotes the number of neighboring joints.

3.2 Text-driven 3D Human and Object Composition

With the help of DreamGaussian (Tang et al., 2023), we efficiently generate the 3D avatar G_h and the 3D object G_o individually based on 3DGS and SDS (discussed in Sec. 3.1). We noticed that even with manual adjustments, such as rescaling and rotating the 3D objects, it's difficult to directly rig the generated 3D human and object models accurately (see Appx. F). Therefore, we strive to seamlessly composite G_h and G_o based on the text prompt in this stage. Specifically, the Gaussian attributes of G_h and G_o would be optimized, as well as three trainable global parameters of G_o, including rotation $\mathcal{R} \in \mathbb{R}^4$, scaling factor $\mathcal{S} \in \mathbb{R}$, and the translation matrix $\mathcal{T} \in \mathbb{R}^3$:

$$\mathbf{X}_{G_o} := \mathcal{S} \cdot (\mathbf{X}_{G_o} \cdot \mathcal{R} + \mathcal{T}), \tag{7}$$

where $\mathbf{X}_{G_o}$ is the set of static Gaussian points.

However, solely utilizing SDS for optimization could frequently lead to disproportionate relationships and erroneous contact areas (see Fig. 3). This issue can be attributed to two potential factors: (1) the absence of emphasis on words describing human-object interaction, which decreases the model's ability to comprehend the relationships between humans and objects; (2) the complexity inherent in human subjects, posing challenges for the diffusion model to identify the most suitable contact areas (see Sec. 4.3).

Spatial-aware SDS (SSDS). Following ComboVerse (Chen et al., 2024b), we employ SSDS to facilitate the compositional 3D generation between the human and the object. Specifically, SSDS augments the SDS with a spatial relationship between the human and the object by scaling the attention maps of the designated tokens <token*> with a constant factor c (where $c > 1$):

$$\texttt{ATT} := \begin{cases} c \cdot \texttt{ATT}_{\texttt{<token>}}, & \text{if} \quad \texttt{<token>} = \texttt{<token*>}, \\ \texttt{ATT}_{\texttt{<token>}}, & \text{otherwise.} \end{cases} \tag{8}$$

Here, <token*> corresponds to the tokens encoding the human-object interaction term, such as <'holding'>, which can be identified through Large Language Models (LLMs) or specified by the user. Consequently, the spatial-aware SDS loss can be written as:

$$\nabla_\theta \mathcal{L}_{\text{SSDS}}(\phi^*, g(\theta)) = \mathbb{E}_{t,\epsilon\sim\mathcal{N}(0,1)} \left[w(t) \left(\epsilon_{\phi^*} \left(\boldsymbol{z}_t; y, t \right) - \epsilon \right) \frac{\partial \boldsymbol{z}}{\partial \boldsymbol{x}} \frac{\partial \boldsymbol{x}}{\partial \theta} \right], \tag{9}$$

where ϕ^* denotes the pre-trained denoising function with the adjusted attention maps.

LLM-guided Contact Retargeting. While spatial-aware SDS could benefit in understanding spatial correlations, it still faces difficulties in identifying the most appropriate contact area (See Fig. 3), which serves as a key component for human-object interaction. According to our studies (see Appx. E for visualization), the diffusion model struggles to accurately estimate contacts, even in the 2D images generated for human-object interaction. To tackle this issue, we propose leveraging Lang-SAM (lan, 2023) to identify the contact area from text prompts. Specifically, starting from the 3D human model G_h, we render it from a frontal viewpoint to produce the image I. This image, alongside textual inputs, undergoes Lang-SAM model to derive 2D segmentation masks $\mathcal{M}$:

$$\texttt{LangSAM}(I, \texttt{<body-part>}) \rightarrow \mathcal{M}, \tag{10}$$

where <body-part> represents the text describing the human body part, such as <'hand'>. Subsequently, we back-project the 2D segmentation labels onto the 3D Gaussians via inverse rendering (Chen et al., 2023c). Specifically, for each pixel u on the segmentation maps, we update the mask value (0 or 1) back to the Gaussians via:

$$w_i = \sum_{i \in \mathcal{N}} o_i(u) \times T_i(u) \times \mathcal{M}(u), \tag{11}$$

where w_i represents the weight of the i-th Gaussian, $\mathcal{N}$ is the collection of Gaussians that can be projected onto the pixel u. $o(\cdot)$, $T(\cdot)$, and $\mathcal{M}(\cdot)$ respectively denote the opacity, transmittance, and segmentation mask value. Following the weight updates, we assess whether a Gaussian corresponds to the segmented region of the human body part by comparing its weight against a pre-defined threshold a. We then initialize the translation parameter $\mathcal{T}$ according to:

$$\mathcal{T} = (\boldsymbol{w}^T * \boldsymbol{\mu}) / \sum \boldsymbol{w}, \tag{12}$$

where $\boldsymbol{w} = \{w_1, ..., w_N | w_i = 0/1\} \in \mathbb{R}^{N\times 1}$, $\boldsymbol{\mu} = \{\mu_1, ..., \mu_N\} \in \mathbb{R}^{N\times 3}$, and N is the number of Gaussain points within the human model G_h.

3.3 Correspondence-aware Motion Field

Following the compositional integration of 3D humans and objects, animating them synchronously presents an additional challenge owing to potential penetration issues. This problem stems from the absence of a well-defined motion field for the object. To this end, we establish the motion fields for both human and object models using the linear blend skinning function from SMPL-X (as in Eq. 6), and propose a correspondence-aware motion optimization aimed at optimizing the trainable global parameters of the object model, *i.e.*, rotation ($\mathcal{R}$) and translation ($\mathcal{T}$), to improve robustness against penetration issues between humans and objects.

Figure 3: **Comparisons on 3D compositional generations.**

Human Animation. Given the motion sequence, we first construct a deformation field, which consists of two components: (1) articulated deformation utilizing the SMPL-X linear blend skinning function $\texttt{LBS}(\cdot)$, and (2) non-rigid motion learning the offset based on HexPlane features (Cao & Johnson, 2023), to deform the point $\mathbf{x}_c$ from the canonical space to $\mathbf{x}_o$ in the observation space:

$$\mathbf{x}_o = \mathcal{G} \cdot \mathbf{x}_c + \texttt{MLP}(F(\mathbf{x}_c, \mathbf{t})), \tag{13}$$

where $F(\cdot)$ denotes the HexPlane-based feature extraction network, and $\mathbf{t}$ indicates the timestamp. We derive $\mathcal{G}$ from the closet canonical SMPL-X vertex to $\mathbf{x}_c$.

Object Animation. Similar to the human animation, we calculate the deformation matrix $\mathcal{G}_c$ for each Gaussian point $\mathbf{x}$ within the object model G_o based on its closest canonical SMPL-X vertex. Given our experimental definition of 3D objects as rigid bodies, we then compute their average to establish the intermediate motion field for the object:

$$\mathbf{X}_o = \mathcal{G}_c^{'} \cdot \mathbf{X}_c, \quad \mathcal{G}_c^{'} = \frac{\sum_{i \in [1,M]} \mathcal{G}_{c_i}}{M}, \tag{14}$$

where $\mathbf{X}_o = \{\mathbf{x}_{o_1}, ..., \mathbf{x}_{o_M}\}$, $\mathbf{X}_c = \{\mathbf{x}_{c_1}, ..., \mathbf{x}_{c_M}\}$, and M is the total number of Gaussian points within G_o. Although animating the object directly using SMPL-X linear blend skinning may seem like a simple solution, it can result in penetration issues between the human and the object (see Fig. 5). This challenge arises primarily from the absence of proper constraints to maintain the correspondence between these two models.

Correspondence-aware Motion Optimization. Drawing insight from the fact that our method is robust in handling penetration issues in static composited models across various scenarios, we propose a correspondence-aware motion optimization to preserve the correspondence between human and object, thereby addressing the penetration problem. Specifically, we extend the above motion field (Eq. 14) to include two additional trainable parameters $\mathcal{R}$ and $\mathcal{T}$:

$$\mathbf{X}_o := \mathbf{X}_o \cdot \mathcal{R} + \mathcal{T}. \tag{15}$$

where $\mathbf{X}_o$ is obtained in Eq. 14. Rather than naïvely optimizing the parameters via SDS, we propose a novel correspondence-aware training objective that leverages SMPL-X as an intermediary to maintain the correspondence between human and object when they are animated to a new pose:

$$\mathcal{L}_{CA} = \text{MSE}(\mathcal{G}_\mathbf{c}, \mathcal{G}_\mathbf{o}), \quad \mathcal{G}_\mathbf{c} = \{\mathcal{G}_{c_0}, ..., \mathcal{G}_{c_M}\}, \quad \mathcal{G}_\mathbf{o} = \{\mathcal{G}_{o_0}, ..., \mathcal{G}_{o_M}\} \tag{16}$$

where $\mathcal{G}_{c_i}$ and $\mathcal{G}_{o_i}$ is respectively derived based on $\mathbf{x}_{c_i}$, $\mathbf{x}_{o_i}$ and their corresponding SMPL-X models.

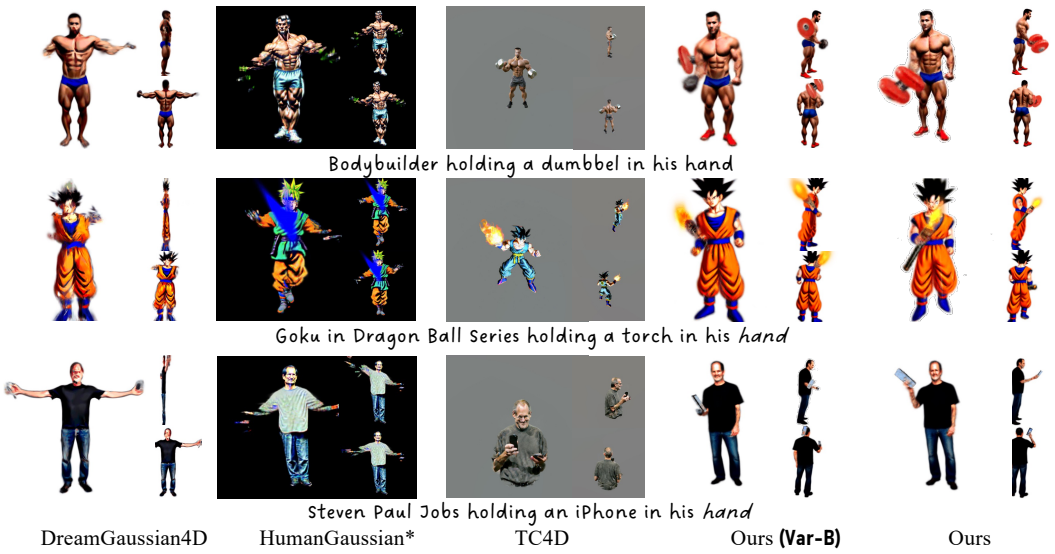

Figure 4: **Comparisons on 4D avatar animation with object interactions.** '$*$' indicates that HumanGaussian directly employs the SMPL LBS function for animation.

In addition to our correspondence-aware loss, we also incorporate the spatial-aware SDS as in Eq. 9 and the texture-structure joint SDS from HumanGaussian (Liu et al., 2023d) to enhance the overall quality:

$$\begin{aligned}\nabla_\theta \mathcal{L}_{\text{SDS}}(\phi, g(\theta)) = \lambda_1 \cdot \mathbb{E}_{t,\epsilon\sim\mathcal{N}(0,1)} \left[w(t) \left(\epsilon_\phi \left(\boldsymbol{z}_{x_t}; y, t \right) - \epsilon_{\boldsymbol{x}} \right) \frac{\partial \boldsymbol{z}_{\boldsymbol{x}}}{\partial \boldsymbol{x}} \frac{\partial \boldsymbol{x}}{\partial \theta} \right] \\ + \lambda_2 \cdot \mathbb{E}_{t,\epsilon\sim\mathcal{N}(0,1)} \left[w(t) \left(\epsilon_\phi \left(\boldsymbol{z}_{d_t}; y, t \right) - \epsilon_{\boldsymbol{d}} \right) \frac{\partial \boldsymbol{z}_{\boldsymbol{d}}}{\partial \boldsymbol{d}} \frac{\partial \boldsymbol{d}}{\partial \theta} \right],\end{aligned} \tag{17}$$

where λ_1 and λ_2 are hyper-parameters to balance the impact of structural and textural losses, while $\boldsymbol{d}$ denotes the depth renderings.

The overall loss function to optimize the 4D animative scene is then given by:

$$\mathcal{L} = \lambda_{CA} \cdot \mathcal{L}_{CA} + \lambda_{\text{SDS}} \cdot \mathcal{L}_{\text{SDS}} + \lambda_{\text{SSDS}} \cdot \mathcal{L}_{\text{SSDS}}, \tag{18}$$

where λ_{CA}, λ_{SDS}, and λ_{SSDS} represents weights to balance the respective losses.

4 Experiments

We now validate the effectiveness and capability of our proposed framework to animate various 3D avatar-object pairs with different poses and provide comparisons with existing 3D and 4D compositional generation methods.

Implementation Details. We follow DreamGaussian4D (Ren et al., 2023) to implement the 3D Gaussian Splatting (Kerbl et al., 2023) and the HexPlane (Cao & Johnson, 2023) in our method. We utilize the pre-trained Texture-Structure joint diffusion model from HumanGaussian (Liu et al., 2023d) and version 2.1 of Stable Diffusion (Stability.AI, 2022) to respectively calculate the SDS and spatial-aware SDS in our implementation. Typically, for each 3D avatar-object pair, we train the 3D stage with a batch size of 16 for 400 epochs, and the 4D stage with a batch size of 10 for 400 epochs. The training takes around 10 minutes for the 3D stage and 20 minutes for the 4D stage on a single NVIDIA A100 GPU. We use Adam (Kingma & Ba, 2015) optimizer for back-propagation. Additional implementation details can be found in the Appx. B.

Comparison Methods for 3D Static Generation. We first compare the 3D static generation results with HumanGaussian (Liu et al., 2023d) and GraphDreamer (Gao et al., 2023). Since ComboVerse (Chen et al., 2024b) lacks an official code release and relies on image inputs, we compare static AvatarGO with an alternative variant, *i.e.*, "Ours (**Var-A**)", by only using the spatial-aware score distillation sampling (SSDS) in ComboVerse to composite 3D humans and avatars. We cannot compare with GALA3D as their source code is not publicly accessible.

Comparison Methods for 4D Animation. Since there are no specific methods tailored for 4D avatar animation with object interactions, we access AvatarGO's efficacy against three recent 4D generation techniques (i.e., DreamGaussian4D (Ren et al., 2023), HumanGaussian (Liu et al., 2023d), and TC4D (Bahmani et al., 2024)), as well as one alternative variant "Ours (**`Var-B`**)". To implement **`Var-B`**, we utilize human hand motion sequences as trajectories to guide the transformation of 3D objects and follow Comp4D to integrate the video diffusion model to compute SDS. Because InterDreamer (Xu et al., 2024b) and InterFusion (Dai et al., 2024) have not released their code, we could not include their results for comparison. See more motivation for designing "Ours (`Var-A`)" and "Ours (`Var-B`)" in Appx. C.

4.1 Qualitative Evaluations

4D Avatar Generation with Object Interaction. In Fig. 1, we present a diverse collection of avatar-object pairs that are animated to different poses. These renderings consistently showcase high-fidelity results from various viewpoints. Thanks to our proposed LLM-guided contact retargeting and correspondence-aware motion optimization, our method can deliver appropriate human-object interactions and demonstrate superior robustness to the penetration issues.

Comparison on 3D Generation. We provide qualitative comparisons with existing methods on 3D generation in Fig. 3. We can observe: 1) without the aid of LLMs, HumanGaussian struggles to determine the spatial correlations between humans and objects; 2) Despite using graphs to establish relationships, GraphDreamer is confused by the meaningful contact, resulting in unsatisfactory outcomes. 3) Optimizing $\mathcal{R}$, $\mathcal{S}$, and $\mathcal{T}$ with only SSDS is inadequate to move the object to the correct area. Conversely, AvatarGO consistently outperforms with precise human-object interactions.

Comparisons on 4D Animation. In Fig. 4, we compare our 4D animation results with SOTA methods. We take the rendering from our 3D compositions stage as the input for DreamGaussian4D. The following observations can be made: 1) Even with human-object interaction images, DreamGaussian4D, which employs video diffusion models, struggles with animating the composited scene. 2) Direct animation via SMPL LBS function, as in HumanGaussian, tends to yield unsmooth results, especially for the arms. 3) TC4D faces similar issues as the DreamGaussian4D. Meanwhile, it treats the entire scene as a single entity, lacking both local and large-scale motions for individual objects. 4) One may think applying trajectory to objects seems like a simple solution (as in Comp4D). However, as seen in "Ours (**`Var-B`**)", it can disrupt spatial correlations between humans and objects. These points further validate the necessity of AvatarGO. Our method can consistently deliver superior results with correct relationships and better robustness to penetration issues See the Appx. A, H, J, K for more comparisons.

4.2 Quantitative Evaluations

CLIP-based Metrics. We use CLIP-based metrics (CLIP-Score (CLIP-S), CLIP image similarity (CLIP-Image), and CLIP Directional Similarity (CLIP-DS) (Brooks et al., 2023; Gal et al., 2022)) with CLIP-ViT-L/14 model. Among them, CLIP-S measures the similarity between texts and their corresponding models, CLIP-Image denotes the similarity between compositional models and human models, and CLIP-DS represents the alignment between changes in text captions (*e.g.*, "Iron Man" to "Iron Man holding an axe of Thor in his hand") and corresponding changes in images. Through Tab. 1, our method maintain the human identity in the composited scenes (see CLIP-Image). Note that "Ours (`Var-A`)" and GraphDreamer is slightly better for this metric as they struggle to do the composition (see Fig. 3). Meanwhile, "Ours" and "Ours (static)" consistently achieve better results than HumanGaussian and other variants, further affirming the objective superiority of AvatarGO.

Table 1: **Quantitative Evaluation.**

	GraphDreamer	TC4D	HumanGaussian	Ours (`Var-A`)	Ours (`Var-B`)	Ours (`static`)	Ours
CLIP-Image ↑	98.44	89.50	83.93	97.88	92.11	**93.45**	92.20
CLIP-S ↑	8.09	19.84	23.69	25.36	30.57	32.27	**32.84**
CLIP-DS ↑	1.71	15.28	4.71	0.91	25.90	**33.80**	28.03

User Studies We further conduct user studies to compare with DreamGaussian4D, HumanGaussian, TC4D, and "Ours (`Var-A`)". 24 Volunteers rated these methods independently based on seven criteria from 1 (worst) to 5 (best): (1) Level of penetration; (2) Accuracy of the relative scale between humans and objects; (3) Accuracy

Table 2: **User studies.**

	Dream Gaussian4D	Human Gaussian	TC4D	Ours (`Var-B`)	Ours
Level of penetration ↑	1.267	1.084	4.236	1.537	**4.872**
Accuracy of relative scale ↑	1.183	1.092	4.308	3.947	**4.788**
Accuracy of contact ↑	1.654	1.137	4.412	2.137	**4.802**
Motion quality ↑	1.321	2.156	1.947	1.673	**4.592**
Motion amount ↑	2.118	3.781	1.517	4.159	**4.934**
Text alignment ↑	2.047	1.918	4.515	2.462	**4.767**
Overall Performance ↑	3.467	1.633	4.033	2.033	**4.869**

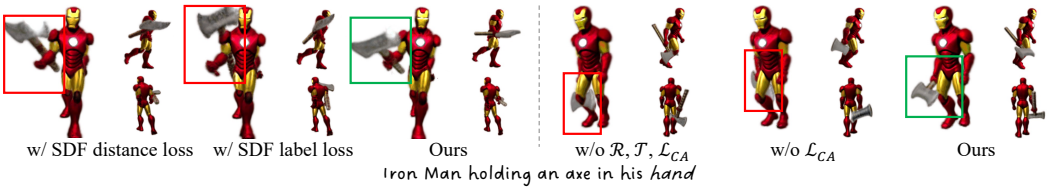

Figure 5: **Analysis of correspondence-aware motion field.**

of contact; (4) Motion quality; (5) Motion amount; (6) Text alignment; (7) Overall performance. Detailed results have been presented in Tab. 2. Key observations include: 1) Both DreamGaussian4D and HumanGaussian have difficulty providing satisfactory outcomes for human-object interaction (HOI) scenes. 2) Although TC4D performs well with HOI generations, it only produces global motions, leading to less optimal motion quality and quantity compared to our method. Our final design consistently delivers superior results for all seven criteria, outperforming the other methods across the board.

4.3 Ablation Studies

Analysis of LLM-guided Contact Retargeting. We first conduct evaluations to validate the efficacy of employing Lang-SAM for retargeting the accurate contact area. See Fig. 3. By comparing "Ours (**`Var-A`**)" and Ours, we can conclude that without Lang-SAM, the model struggles to produce correct human-object interaction in the 3D compositional generation.

Analysis of Correspondence-aware Motion Field. In Fig. 5, we first compare our proposed training objectives $\mathcal{L}_{CA}$ with two alternative strategies: 1) "SDF distance loss" which minimizes the change of signed distance field (SDF) between objects and humans when they are animated to a new pose, and 2) "SDF label loss" that supervise the label of SDF instead. These comparisons demonstrate the effectiveness of our proposed method for maintaining spatial correlations during the animations. Additionally, we validate our model's design by further comparing it with two variants: 1) "w/o $\mathcal{R}$, $\mathcal{T}$, $\mathcal{L}_{CA}$" which disables the trainable parameters $\mathcal{R}$, $\mathcal{T}$, Eq. 15, and our proposed loss $\mathcal{L}_{CA}$. This setting represents the scenario where the object is moved directly with the contact point. and 2) "w/o $\mathcal{L}_{CA}$" which trains the animation network solely with SDS loss ($\mathcal{L}^*_{SDS}$, $\mathcal{L}_{SDS}$). These comparisons underscore the necessity of these components in achieving 4D animation with better robustness to the penetration issues.

Analysis of Spatial-aware SDS. We finally assess the effectiveness of spatial-aware SDS (SSDS) and present the results in Fig. 6. Notably, we observe that SSDS plays a crucial role in preventing the optimization of $\mathcal{R}$, $\mathcal{S}$, $\mathcal{T}$ from vanishing during 3D compositional generation. Additionally, there is a drop in the quality of the animated avatars when disabling SSDS.

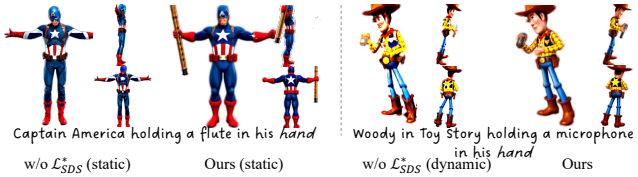

Figure 6: **Analysis of Spatial-aware SDS.**

5 Conclusions

In this paper, we have introduced AvatarGO, the first attempt for text-guided 4D avatar generation with object interactions. Within AvatarGO, we proposed to employ large language model for comprehending the most suitable contact area between humans and objects. We also presented a novel correspondence-aware motion optimization that utilizes SMPL-X as an intermediary to enhance the model's resilience to penetration issues when animating 3D humans and objects into new poses. Extensive evaluations demonstrated that our method has achieved high-fidelity 4D animations across diverse 3D avatar-object pairs and poses, surpassing current state-of-the-arts by a large margin.

Limitations. While opening new doors for human-centric 4D content generation, we acknowledge AvatarGO has certain limitations: 1) Our pipeline operates under the assumption of rigid-body dynamics for 3D objects, making it unsuitable for animating non-rigid content such as flags; 2) our method presumes that continuous contact between objects and avatars, making it challenges for tasks like "Dribbling the basketball," where the human and object inevitably disconnect at certain points. Nevertheless, our current approach does not cover all possible scenarios, it effectively handles continuous contact and rigid connections, which are commonly encountered in real-world applications.

REFERENCES

Language segment anything. https://github.com/paulguerrero/lang-sam.git, 2023. 3, 6

Sherwin Bahmani, Ivan Skorokhodov, Victor Rong, Gordon Wetzstein, Leonidas Guibas, Peter Wonka, Sergey Tulyakov, Jeong Joon Park, Andrea Tagliasacchi, and David B Lindell. 4d-fy: Text-to-4d generation using hybrid score distillation sampling. *arXiv preprint arXiv:2311.17984*, 2023. 3

Sherwin Bahmani, Xian Liu, Yifan Wang, Ivan Skorokhodov, Victor Rong, Ziwei Liu, Xihui Liu, Jeong Joon Park, Sergey Tulyakov, Gordon Wetzstein, et al. Tc4d: Trajectory-conditioned text-to-4d generation. *arXiv preprint arXiv:2403.17920*, 2024. 2, 4, 9, 19

Yogesh Balaji, Seungjun Nah, Xun Huang, Arash Vahdat, Jiaming Song, Karsten Kreis, Miika Aittala, Timo Aila, Samuli Laine, Bryan Catanzaro, et al. ediffi: Text-to-image diffusion models with an ensemble of expert denoisers. *arXiv preprint arXiv:2211.01324*, 2022. 1, 3

Bharat Lal Bhatnagar, Xianghui Xie, Ilya Petrov, Cristian Sminchisescu, Christian Theobalt, and Gerard Pons-Moll. Behave: Dataset and method for tracking human object interactions. In *IEEE Conference on Computer Vision and Pattern Recognition (CVPR)*. IEEE, jun 2022. 1

Andreas Blattmann, Tim Dockhorn, Sumith Kulal, Daniel Mendelevitch, Maciej Kilian, Dominik Lorenz, Yam Levi, Zion English, Vikram Voleti, Adam Letts, et al. Stable video diffusion: Scaling latent video diffusion models to large datasets. *arXiv preprint arXiv:2311.15127*, 2023. 2

Tim Brooks, Aleksander Holynski, and Alexei A Efros. Instructpix2pix: Learning to follow image editing instructions. In *IEEE Conference on Computer Vision and Pattern Recognition*, 2023. 9

Ang Cao and Justin Johnson. Hexplane: A fast representation for dynamic scenes. In *Proceedings of the IEEE/CVF Conference on Computer Vision and Pattern Recognition*, pp. 130–141, 2023. 7, 8, 18

Tianshi Cao, Karsten Kreis, Sanja Fidler, Nicholas Sharp, and Kangxue Yin. Texfusion: Synthesizing 3d textures with text-guided image diffusion models. In *Proceedings of the IEEE/CVF International Conference on Computer Vision*, pp. 4169–4181, 2023a. 3

Yukang Cao, Yan-Pei Cao, Kai Han, Ying Shan, and Kwan-Yee K Wong. Dreamavatar: Text-and-shape guided 3d human avatar generation via diffusion models. *arXiv preprint arXiv:2304.00916*, 2023b. 1, 3

Yukang Cao, Yan-Pei Cao, Kai Han, Ying Shan, and Kwan-Yee K Wong. Guide3d: Create 3d avatars from text and image guidance. *arXiv preprint arXiv:2308.09705*, 2023c. 3

Mathilde Caron, Hugo Touvron, Ishan Misra, Hervé Jégou, Julien Mairal, Piotr Bojanowski, and Armand Joulin. Emerging properties in self-supervised vision transformers. In *Proceedings of the IEEE/CVF international conference on computer vision*, pp. 9650–9660, 2021. 3

Dave Zhenyu Chen, Yawar Siddiqui, Hsin-Ying Lee, Sergey Tulyakov, and Matthias Nießner. Text2tex: Text-driven texture synthesis via diffusion models. *arXiv preprint arXiv:2303.11396*, 2023a. 3

Rui Chen, Yongwei Chen, Ningxin Jiao, and Kui Jia. Fantasia3d: Disentangling geometry and appearance for high-quality text-to-3d content creation. *arXiv preprint arXiv:2303.13873*, 2023b. 3

Rui Chen, Mingyi Shi, Shaoli Huang, Ping Tan, Taku Komura, and Xuelin Chen. Taming diffusion probabilistic models for character control. In *SIGGRAPH*, 2024a. 1

Yiwen Chen, Zilong Chen, Chi Zhang, Feng Wang, Xiaofeng Yang, Yikai Wang, Zhongang Cai, Lei Yang, Huaping Liu, and Guosheng Lin. Gaussianeditor: Swift and controllable 3d editing with gaussian splatting. *arXiv preprint arXiv:2311.14521*, 2023c. 6

Yongwei Chen, Tengfei Wang, Tong Wu, Xingang Pan, Kui Jia, and Ziwei Liu. Comboverse: Compositional 3d assets creation using spatially-aware diffusion guidance. *arXiv preprint arXiv:2403.12409*, 2024b. 2, 3, 6, 8

Sisi Dai, Wenhao Li, Haowen Sun, Haibin Huang, Chongyang Ma, Hui Huang, Kai Xu, and Ruizhen Hu. Interfusion: Text-driven generation of 3d human-object interaction. *arXiv preprint arXiv:2403.15612*, 2024. 2, 3, 9

Matt Deitke, Dustin Schwenk, Jordi Salvador, Luca Weihs, Oscar Michel, Eli VanderBilt, Ludwig Schmidt, Kiana Ehsani, Aniruddha Kembhavi, and Ali Farhadi. Objaverse: A universe of annotated 3d objects. In *Proceedings of the IEEE/CVF Conference on Computer Vision and Pattern Recognition*, pp. 13142–13153, 2023. 3

Matt Deitke, Ruoshi Liu, Matthew Wallingford, Huong Ngo, Oscar Michel, Aditya Kusupati, Alan Fan, Christian Laforte, Vikram Voleti, Samir Yitzhak Gadre, et al. Objaverse-xl: A universe of 10m+ 3d objects. *Advances in Neural Information Processing Systems*, 36, 2024. 3

Dave Epstein, Ben Poole, Ben Mildenhall, Alexei A Efros, and Aleksander Holynski. Disentangled 3d scene generation with layout learning. *arXiv preprint arXiv:2402.16936*, 2024. 2, 3

Rinon Gal, Or Patashnik, Haggai Maron, Amit H Bermano, Gal Chechik, and Daniel Cohen-Or. Stylegan-nada: Clip-guided domain adaptation of image generators. *ACM Transactions on Graphics (TOG)*, 2022. 9

Gege Gao, Weiyang Liu, Anpei Chen, Andreas Geiger, and Bernhard Schölkopf. Graphdreamer: Compositional 3d scene synthesis from scene graphs. *arXiv preprint arXiv:2312.00093*, 2023. 1, 3, 8, 19, 22

Xun Guo, Mingwu Zheng, Liang Hou, Yuan Gao, Yufan Deng, Chongyang Ma, Weiming Hu, Zhengjun Zha, Haibin Huang, Pengfei Wan, et al. I2v-adapter: A general image-to-video adapter for video diffusion models. *arXiv preprint arXiv:2312.16693*, 2023a. 2

Yuan-Chen Guo, Ying-Tian Liu, Ruizhi Shao, Christian Laforte, Vikram Voleti, Guan Luo, Chia-Hao Chen, Zi-Xin Zou, Chen Wang, Yan-Pei Cao, and Song-Hai Zhang. threestudio: A unified framework for 3d content generation. https://github.com/threestudio-project/threestudio, 2023b. 17, 18

Kaiming He, Xiangyu Zhang, Shaoqing Ren, and Jian Sun. Deep residual learning for image recognition. In *IEEE Conference on Computer Vision and Pattern Recognition*, 2016. 18

Fangzhou Hong, Jiaxiang Tang, Ziang Cao, Min Shi, Tong Wu, Zhaoxi Chen, Tengfei Wang, Liang Pan, Dahua Lin, and Ziwei Liu. 3dtopia: Large text-to-3d generation model with hybrid diffusion priors. *arXiv preprint arXiv:2403.02234*, 2024. 3

Yicong Hong, Kai Zhang, Jiuxiang Gu, Sai Bi, Yang Zhou, Difan Liu, Feng Liu, Kalyan Sunkavalli, Trung Bui, and Hao Tan. Lrm: Large reconstruction model for single image to 3d. *arXiv preprint arXiv:2311.04400*, 2023. 3

Xin Huang, Ruizhi Shao, Qi Zhang, Hongwen Zhang, Ying Feng, Yebin Liu, and Qing Wang. Humannorm: Learning normal diffusion model for high-quality and realistic 3d human generation. *arXiv preprint arXiv:2310.01406*, 2023a. 3

Yukun Huang, Jianan Wang, Ailing Zeng, He Cao, Xianbiao Qi, Yukai Shi, Zheng-Jun Zha, and Lei Zhang. Dreamwaltz: Make a scene with complex 3d animatable avatars. *arXiv preprint arXiv:2305.12529*, 2023b. 3

Zhewei Huang, Tianyuan Zhang, Wen Heng, Boxin Shi, and Shuchang Zhou. Real-time intermediate flow estimation for video frame interpolation. In *European Conference on Computer Vision*, pp. 624–642. Springer, 2022. 4

Nan Jiang, Tengyu Liu, Zhexuan Cao, Jieming Cui, Zhiyuan Zhang, Yixin Chen, He Wang, Yixin Zhu, and Siyuan Huang. Full-body articulated human-object interaction. In *Proceedings of the IEEE/CVF International Conference on Computer Vision*, pp. 9365–9376, 2023a. 1

Ruixiang Jiang, Can Wang, Jingbo Zhang, Menglei Chai, Mingming He, Dongdong Chen, and Jing Liao. Avatarcraft: Transforming text into neural human avatars with parameterized shape and pose control. *arXiv preprint arXiv:2303.17606*, 2023b. 3

Yanqin Jiang, Li Zhang, Jin Gao, Weimin Hu, and Yao Yao. Consistent4d: Consistent 360 {\deg} dynamic object generation from monocular video. *arXiv preprint arXiv:2311.02848*, 2023c. 4

Roy Kapon, Guy Tevet, Daniel Cohen-Or, and Amit H Bermano. Mas: Multi-view ancestral sampling for 3d motion generation using 2d diffusion. In *Proceedings of the IEEE/CVF Conference on Computer Vision and Pattern Recognition*, pp. 1965–1974, 2024. 1

Bernhard Kerbl, Georgios Kopanas, Thomas Leimkühler, and George Drettakis. 3d gaussian splatting for real-time radiance field rendering. *ACM Transactions on Graphics (ToG)*, 42(4):1–14, 2023. 3, 4, 8

Diederik P Kingma and Jimmy Ba. Adam: A method for stochastic optimization. In *International Conference on Learning Representations*, 2015. 8

Nikos Kolotouros, Thiemo Alldieck, Andrei Zanfir, Eduard Gabriel Bazavan, Mihai Fieraru, and Cristian Sminchisescu. Dreamhuman: Animatable 3d avatars from text. *arXiv preprint arXiv:2306.09329*, 2023. 3

Jiahao Li, Hao Tan, Kai Zhang, Zexiang Xu, Fujun Luan, Yinghao Xu, Yicong Hong, Kalyan Sunkavalli, Greg Shakhnarovich, and Sai Bi. Instant3d: Fast text-to-3d with sparse-view generation and large reconstruction model. *arXiv preprint arXiv:2311.06214*, 2023a. 3

Jiaman Li, Jiajun Wu, and C Karen Liu. Object motion guided human motion synthesis. *ACM Trans. Graph.*, 42(6), 2023b. 1

Tingting Liao, Hongwei Yi, Yuliang Xiu, Jiaxaing Tang, Yangyi Huang, Justus Thies, and Michael J Black. Tada! text to animatable digital avatars. *arXiv preprint arXiv:2308.10899*, 2023. 1, 3

Chen-Hsuan Lin, Jun Gao, Luming Tang, Towaki Takikawa, Xiaohui Zeng, Xun Huang, Karsten Kreis, Sanja Fidler, Ming-Yu Liu, and Tsung-Yi Lin. Magic3d: High-resolution text-to-3d content creation. In *IEEE Conference on Computer Vision and Pattern Recognition*, 2023. 1, 3

Fangfu Liu, Hanyang Wang, Weiliang Chen, Haowen Sun, and Yueqi Duan. Make-your-3d: Fast and consistent subject-driven 3d content generation. *arXiv preprint arXiv:2403.09625*, 2024. 3

Minghua Liu, Ruoxi Shi, Linghao Chen, Zhuoyang Zhang, Chao Xu, Xinyue Wei, Hansheng Chen, Chong Zeng, Jiayuan Gu, and Hao Su. One-2-3-45++: Fast single image to 3d objects with consistent multi-view generation and 3d diffusion. *arXiv preprint arXiv:2311.07885*, 2023a. 3

Minghua Liu, Chao Xu, Haian Jin, Linghao Chen, Zexiang Xu, Hao Su, et al. One-2-3-45: Any single image to 3d mesh in 45 seconds without per-shape optimization. *arXiv preprint arXiv:2306.16928*, 2023b. 3

Ruoshi Liu, Rundi Wu, Basile Van Hoorick, Pavel Tokmakov, Sergey Zakharov, and Carl Vondrick. Zero-1-to-3: Zero-shot one image to 3d object. In *Proceedings of the IEEE/CVF International Conference on Computer Vision*, pp. 9298–9309, 2023c. 1, 3

Xian Liu, Xiaohang Zhan, Jiaxiang Tang, Ying Shan, Gang Zeng, Dahua Lin, Xihui Liu, and Ziwei Liu. Humangaussian: Text-driven 3d human generation with gaussian splatting. *arXiv preprint arXiv:2311.17061*, 2023d. 2, 8, 9, 19, 22, 23

Yuan Liu, Cheng Lin, Zijiao Zeng, Xiaoxiao Long, Lingjie Liu, Taku Komura, and Wenping Wang. Syncdreamer: Generating multiview-consistent images from a single-view image. *arXiv preprint arXiv:2309.03453*, 2023e. 3

Zexiang Liu, Yangguang Li, Youtian Lin, Xin Yu, Sida Peng, Yan-Pei Cao, Xiaojuan Qi, Xiaoshui Huang, Ding Liang, and Wanli Ouyang. Unidream: Unifying diffusion priors for relightable text-to-3d generation. *arXiv preprint arXiv:2312.08754*, 2023f. 3

Xiaoxiao Long, Yuan-Chen Guo, Cheng Lin, Yuan Liu, Zhiyang Dou, Lingjie Liu, Yuexin Ma, Song-Hai Zhang, Marc Habermann, Christian Theobalt, et al. Wonder3d: Single image to 3d using cross-domain diffusion. *arXiv preprint arXiv:2310.15008*, 2023. 3

Matthew Loper, Naureen Mahmood, Javier Romero, Gerard Pons-Moll, and Michael J. Black. SMPL: A skinned multi-person linear model. *ACM Trans. Graphics, Asia*, 2015. 1, 5

Gal Metzer, Elad Richardson, Or Patashnik, Raja Giryes, and Daniel Cohen-Or. Latent-nerf for shape-guided generation of 3d shapes and textures. *arXiv preprint arXiv:2211.07600*, 2022. 3

Ben Mildenhall, Pratul P Srinivasan, Matthew Tancik, Jonathan T Barron, Ravi Ramamoorthi, and Ren Ng. Nerf: Representing scenes as neural radiance fields for view synthesis. In *European Conference on Computer Vision*, 2020. 3

Maxime Oquab, Timothée Darcet, Théo Moutakanni, Huy Vo, Marc Szafraniec, Vasil Khalidov, Pierre Fernandez, Daniel Haziza, Francisco Massa, Alaaeldin El-Nouby, et al. Dinov2: Learning robust visual features without supervision. *arXiv preprint arXiv:2304.07193*, 2023. 3

Georgios Pavlakos, Vasileios Choutas, Nima Ghorbani, Timo Bolkart, Ahmed A. A. Osman, Dimitrios Tzionas, and Michael J. Black. Expressive body capture: 3d hands, face, and body from a single image. In *IEEE Conference on Computer Vision and Pattern Recognition*, 2019. 1, 5

Ben Poole, Ajay Jain, Jonathan T. Barron, and Ben Mildenhall. Dreamfusion: Text-to-3d using 2d diffusion. In *International Conference on Learning Representations*, 2022. 1

Aditya Ramesh, Prafulla Dhariwal, Alex Nichol, Casey Chu, and Mark Chen. Hierarchical text-conditional image generation with clip latents. *arXiv preprint arXiv:2204.06125*, 2022. 1, 3

Jiawei Ren, Liang Pan, Jiaxiang Tang, Chi Zhang, Ang Cao, Gang Zeng, and Ziwei Liu. Dreamgaussian4d: Generative 4d gaussian splatting. *arXiv preprint arXiv:2312.17142*, 2023. 2, 4, 8, 9, 17, 19, 23

Elad Richardson, Gal Metzer, Yuval Alaluf, Raja Giryes, and Daniel Cohen-Or. Texture: Text-guided texturing of 3d shapes. *arXiv preprint arXiv:2302.01721*, 2023. 3

Chitwan Saharia, William Chan, Saurabh Saxena, Lala Li, Jay Whang, Emily Denton, Seyed Kamyar Seyed Ghasemipour, Burcu Karagol Ayan, S Sara Mahdavi, Rapha Gontijo Lopes, et al. Photorealistic text-to-image diffusion models with deep language understanding. *arXiv preprint arXiv:2205.11487*, 2022. 1, 3

Junyoung Seo, Wooseok Jang, Min-Seop Kwak, Jaehoon Ko, Hyeonsu Kim, Junho Kim, Jin-Hwa Kim, Jiyoung Lee, and Seungryong Kim. Let 2d diffusion model know 3d-consistency for robust text-to-3d generation. *arXiv preprint arXiv:2303.07937*, 2023. 3

Yonatan Shafir, Guy Tevet, Roy Kapon, and Amit H Bermano. Human motion diffusion as a generative prior. *arXiv preprint arXiv:2303.01418*, 2023. 1

Tianchang Shen, Jun Gao, Kangxue Yin, Ming-Yu Liu, and Sanja Fidler. Deep marching tetrahedra: a hybrid representation for high-resolution 3d shape synthesis. In *Advances in Neural Information Processing Systems*, 2021. 3

Tianchang Shen, Jacob Munkberg, Jon Hasselgren, Kangxue Yin, Zian Wang, Wenzheng Chen, Zan Gojcic, Sanja Fidler, Nicholas Sharp, and Jun Gao. Flexible isosurface extraction for gradient-based mesh optimization. *ACM Transactions on Graphics (TOG)*, 42(4):1–16, 2023. 3

Ruoxi Shi, Hansheng Chen, Zhuoyang Zhang, Minghua Liu, Chao Xu, Xinyue Wei, Linghao Chen, Chong Zeng, and Hao Su. Zero123++: a single image to consistent multi-view diffusion base model. *arXiv preprint arXiv:2310.15110*, 2023a. 3

Yichun Shi, Peng Wang, Jianglong Ye, Long Mai, Kejie Li, and Xiao Yang. Mvdream: Multi-view diffusion for 3d generation. *arXiv:2308.16512*, 2023b. 3

Uriel Singer, Shelly Sheynin, Adam Polyak, Oron Ashual, Iurii Makarov, Filippos Kokkinos, Naman Goyal, Andrea Vedaldi, Devi Parikh, Justin Johnson, et al. Text-to-4d dynamic scene generation. *arXiv preprint arXiv:2301.11280*, 2023. 3

Stability.AI. Stable diffusion. https://stability.ai/blog/stable-diffusion-public-release, 2022. 1, 3, 8

Stability.AI. Stability AI releases DeepFloyd IF, a powerful text-to-image model that can smartly integrate text into images. https://stability.ai/blog/deepfloyd-if-text-to-image-model, 2023. 1, 3

Jiaxiang Tang, Jiawei Ren, Hang Zhou, Ziwei Liu, and Gang Zeng. Dreamgaussian: Generative gaussian splatting for efficient 3d content creation. *arXiv preprint arXiv:2309.16653*, 2023. 1, 2, 3, 4, 5

Jiaxiang Tang, Zhaoxi Chen, Xiaokang Chen, Tengfei Wang, Gang Zeng, and Ziwei Liu. Lgm: Large multi-view gaussian model for high-resolution 3d content creation. *arXiv preprint arXiv:2402.05054*, 2024a. 3

Jiaxiang Tang, Ruijie Lu, Xiaokang Chen, Xiang Wen, Gang Zeng, and Ziwei Liu. Intex: Interactive text-to-texture synthesis via unified depth-aware inpainting. *arXiv preprint arXiv:2403.11878*, 2024b. 3

Shitao Tang, Jiacheng Chen, Dilin Wang, Chengzhou Tang, Fuyang Zhang, Yuchen Fan, Vikas Chandra, Yasutaka Furukawa, and Rakesh Ranjan. Mvdiffusion++: A dense high-resolution multi-view diffusion model for single or sparse-view 3d object reconstruction. *arXiv preprint arXiv:2402.12712*, 2024c. 3

Ashish Vaswani, Noam Shazeer, Niki Parmar, Jakob Uszkoreit, Llion Jones, Aidan N Gomez, Łukasz Kaiser, and Illia Polosukhin. Attention is all you need. *Advances in neural information processing systems*, 30, 2017. 3

Peihao Wang, Zhiwen Fan, Dejia Xu, Dilin Wang, Sreyas Mohan, Forrest Iandola, Rakesh Ranjan, Yilei Li, Qiang Liu, Zhangyang Wang, et al. Steindreamer: Variance reduction for text-to-3d score distillation via stein identity. *arXiv preprint arXiv:2401.00604*, 2023a. 3

Peng Wang, Hao Tan, Sai Bi, Yinghao Xu, Fujun Luan, Kalyan Sunkavalli, Wenping Wang, Zexiang Xu, and Kai Zhang. Pf-lrm: Pose-free large reconstruction model for joint pose and shape prediction. *arXiv preprint arXiv:2311.12024*, 2023b. 3

Xinzhou Wang, Yikai Wang, Junliang Ye, Zhengyi Wang, Fuchun Sun, Pengkun Liu, Ling Wang, Kai Sun, Xintong Wang, and Bin He. Animatabledreamer: Text-guided non-rigid 3d model generation and reconstruction with canonical score distillation. *arXiv preprint arXiv:2312.03795*, 2023c. 4

Zhengyi Wang, Cheng Lu, Yikai Wang, Fan Bao, Chongxuan Li, Hang Su, and Jun Zhu. Prolificdreamer: High-fidelity and diverse text-to-3d generation with variational score distillation. *arXiv preprint arXiv:2305.16213*, 2023d. 1, 3

Zhengyi Wang, Yikai Wang, Yifei Chen, Chendong Xiang, Shuo Chen, Dajiang Yu, Chongxuan Li, Hang Su, and Jun Zhu. Crm: Single image to 3d textured mesh with convolutional reconstruction model. *arXiv preprint arXiv:2403.05034*, 2024. 3

Tianyu Wu, Shizhu He, Jingping Liu, Siqi Sun, Kang Liu, Qing-Long Han, and Yang Tang. A brief overview of chatgpt: The history, status quo and potential future development. *IEEE/CAA Journal of Automatica Sinica*, 10(5):1122–1136, 2023a. 1

Tong Wu, Jiarui Zhang, Xiao Fu, Yuxin Wang, Jiawei Ren, Liang Pan, Wayne Wu, Lei Yang, Jiaqi Wang, Chen Qian, et al. Omniobject3d: Large-vocabulary 3d object dataset for realistic perception, reconstruction and generation. In *Proceedings of the IEEE/CVF Conference on Computer Vision and Pattern Recognition*, pp. 803–814, 2023b. 3

Zike Wu, Pan Zhou, Xuanyu Yi, Xiaoding Yuan, and Hanwang Zhang. Consistent3d: Towards consistent high-fidelity text-to-3d generation with deterministic sampling prior. *arXiv preprint arXiv:2401.09050*, 2024. 3

Dejia Xu, Hanwen Liang, Neel P Bhatt, Hezhen Hu, Hanxue Liang, Konstantinos N Plataniotis, and Zhangyang Wang. Comp4d: Llm-guided compositional 4d scene generation. *arXiv preprint arXiv:2403.16993*, 2024a. 2, 4, 18

Sirui Xu, Ziyin Wang, Yu-Xiong Wang, and Liang-Yan Gui. Interdreamer: Zero-shot text to 3d dynamic human-object interaction. *arXiv preprint arXiv:2403.19652*, 2024b. 1, 9

Yinghao Xu, Hao Tan, Fujun Luan, Sai Bi, Peng Wang, Jiahao Li, Zifan Shi, Kalyan Sunkavalli, Gordon Wetzstein, Zexiang Xu, et al. Dmv3d: Denoising multi-view diffusion using 3d large reconstruction model. *arXiv preprint arXiv:2311.09217*, 2023. 3

Yuyang Yin, Dejia Xu, Zhangyang Wang, Yao Zhao, and Yunchao Wei. 4dgen: Grounded 4d content generation with spatial-temporal consistency. *arXiv preprint arXiv:2312.17225*, 2023. 4

Xu Yinghao, Shi Zifan, Yifan Wang, Chen Hansheng, Yang Ceyuan, Peng Sida, Shen Yujun, and Wetzstein Gordon. Grm: Large gaussian reconstruction model for efficient 3d reconstruction and generation, 2024. 3

Ye Yuan, Xueting Li, Yangyi Huang, Shalini De Mello, Koki Nagano, Jan Kautz, and Umar Iqbal. Gavatar: Animatable 3d gaussian avatars with implicit mesh learning. *arXiv preprint arXiv:2312.11461*, 2023. 4

Yifei Zeng, Yuanxun Lu, Xinya Ji, Yao Yao, Hao Zhu, and Xun Cao. Avatarbooth: High-quality and customizable 3d human avatar generation. *arXiv preprint arXiv:2306.09864*, 2023. 3

Lvmin Zhang and Maneesh Agrawala. Adding conditional control to text-to-image diffusion models. *arXiv preprint arXiv:2302.05543*, 2023. 19

Mingyuan Zhang, Zhongang Cai, Liang Pan, Fangzhou Hong, Xinying Guo, Lei Yang, and Ziwei Liu. Motiondiffuse: Text-driven human motion generation with diffusion model. *arXiv preprint arXiv:2208.15001*, 2022. 1

Mingyuan Zhang, Xinying Guo, Liang Pan, Zhongang Cai, Fangzhou Hong, Huirong Li, Lei Yang, and Ziwei Liu. Remodiffuse: Retrieval-augmented motion diffusion model. In *Proceedings of the IEEE/CVF International Conference on Computer Vision*, pp. 364–373, 2023. 1, 2

Mingyuan Zhang, Daisheng Jin, Chenyang Gu, Fangzhou Hong, Zhongang Cai, Jingfang Huang, Chongzhi Zhang, Xinying Guo, Lei Yang, Ying He, et al. Large motion model for unified multi-modal motion generation. *arXiv preprint arXiv:2404.01284*, 2024. 1, 2

Yufeng Zheng, Xueting Li, Koki Nagano, Sifei Liu, Otmar Hilliges, and Shalini De Mello. A unified approach for text-and image-guided 4d scene generation. *arXiv preprint arXiv:2311.16854*, 2023. 4

Xiaoyu Zhou, Xingjian Ran, Yajiao Xiong, Jinlin He, Zhiwei Lin, Yongtao Wang, Deqing Sun, and Ming-Hsuan Yang. Gala3d: Towards text-to-3d complex scene generation via layout-guided generative gaussian splatting. *arXiv preprint arXiv:2402.07207*, 2024. 2, 3

A VIDEO RESULTS

To better visualize the generated results, we offer an improved demonstration of our method through rotated videos in the supplementary materials. To access this demonstration, please open the file named **"index.html"** provided in the supplementary.

B IMPLEMENTATION DETAILS

Our network is built upon the official implementation of DreamGaussian4D (Ren et al., 2023) and Threestudio (Guo et al., 2023b) (an open-source 3D generative project).

To ensure easy reproducibility, we first include all the hyperparameters for our 3D composition stage in Tab. 3.

Table 3: **Hyper-parameters of AvatarGO - 3D composition stage.**

Camera setting	Camera distance range	2.
	Radius	2.0
	Elevation range	(-30, 30)
	FoV range	49.1
Render setting	Resolution for 0-120 epochs	(128, 128)
	Resolution for 120-240 iters	(256, 256)
	Resolution for 240-400 iters	(512, 512)
Diffusion setting	Guidance scale	7.5
	t range	(0.01, 0.97)
	Minimal step percent	0.01
	Maximal step percent	0.97
	$\omega(t)$	$\sqrt{\alpha_t}(1-\alpha_t)$
Initialization	Rotation $\mathcal{R}$	torch.normal(mean=[0.5, 0.5, 0.5, 0.5], std=0.1)
	Translation $\mathcal{T}$	0.0
	Scale $\mathcal{S}$	torch.normal(mean=1.0, std=0.3)
Learning rate	Rotation $\mathcal{R}$	0.005
	Translation $\mathcal{T}$	0.005
	Scale $\mathcal{S}$	0.005
LLM-guided contact retargeting	threshold a	1e-7
Training objectives	λ^*_{SDS}	1.0
Hardware	GPU	1 × NVIDIA A100 (80GB)

Table 4: **Hyper-parameters of AvatarGO - 4D animataion stage.**

Camera setting	Camera distance range	2.
	Radius	2.0
	Elevation range	(-30, 30)
	FoV range	49.1
Render setting	Resolution for 0-120 epochs	(128, 128)
	Resolution for 120-240 iters	(256, 256)
	Resolution for 240-400 iters	(512, 512)
Diffusion setting to calculate $\mathcal{L}^*_{SDS}$	Guidance scale	7.5
	t range	(0.01, 0.97)
	Minimal step percent	0.01
	Maximal step percent	0.97
	$\omega(t)$	$\sqrt{\alpha_t}(1-\alpha_t)$
Diffusion setting to calculate $\mathcal{L}_{SDS}$	Guidance scale	7.5
	Guidance rescale	0.75
	t range	(0.02, 0.98)
	Minimal step percent	0.02
	Maximal step percent	0.98
	gradient clip	[0, 1.5, 2.0, 1000]
	gradient clip pixel	True
	gradient clip threshold	1.0
	$\omega(t)$	$\sqrt{\alpha_t}(1-\alpha_t)$
Initialization	Rotation $\mathcal{R}$	[-0.16, -0.16, -0.16, 0.5]
	Translation $\mathcal{T}$	0.0
Learning rate	Rotation $\mathcal{R}$	0.001
	Translation $\mathcal{T}$	0.001
Training objectives	λ_{CA}	1e+3
	λ^*_{SDS}	1.0
	λ_{SDS}	1.0
Hardware	GPU	1 × NVIDIA A100 (80GB)

In the 4D animation stage, we apply HexPlane (Cao & Johnson, 2023) to produce features from point position $\mathbf{x}_c$ and timestamp $\mathbf{t}$, followed by an MLP to predict the offset for Gaussian attributes, i.e., point location $\mathbf{x}$, scaling matrix s, rotation matrix R. Specifically, the HexPlane encoder lifts the inputs to a higher frequency dimension $F((\mathbf{x}_c, \mathbf{t})) \in \mathbb{R}^{128}$, while the MLP is set to the default in DreamGaussian4D with ResNet (He et al., 2016).

To further ensure easy reproducibility, we first include all the hyperparameters for our 4D animation stage in Tab. 4 The other hyper-parameters are set to be the default of DreamGaussian4D (Guo et al., 2023b).

C More explanation on designing "Ours (Var-A)" and "Ours (Var-B)"

"Ours (Var-A)": This is a version where we have disabled the Lang-SAM initialization in our 3D static compositional generation. Comparing this with our final method shows that without assistance from Lang-SAM, the diffusion model struggles to accurately interpret human-object images.

"Ours (Var-B)": While Comp4D (Xu et al., 2024a) separates 3D scenes into two components and applies trajectories to one component for compositional 4D generation, it leaves the other component static. This method is not suitable for our scenarios where both humans and objects are dynamic. Therefore, we design "Ours (Var-B)" by adopting the Comp4D strategy: allowing the object to follow a trajectory while the human moves independently. Specifically, we replace our correspondence-aware motion supervision, as defined in Eq. 16, with SDS supervision strategy via the video diffusion model used in Comp4D. Comparing this approach with our final method demonstrates that our correspondence-aware motion supervision more effectively preserves the relationship between humans and objects throughout the animation process.

D TRAINING COMPLEXITY

In our study, our results, detailed in both the main paper and the Appendix, involve training the 3D stage for 400 epochs on a single NVIDIA A100 GPU, taking approximately 10 minutes. Similarly, the 4D stage requires roughly 20 minutes of training on the same GPU. To compare with other methods: 1) In the experiments for 3D compositional generation, HumanGaussian (Liu et al., 2023d) demands approximately 2 hours to complete 3600 epochs; GraphDreamer (Gao et al., 2023) adopts a two-stage training approach, with the coarse stage taking roughly 3 hours for 10000 epochs and the fine stage requiring around 6 hours for 20000 epochs. 2) Additionally, in our experiments with 4D animation, DreamGaussian4D (Ren et al., 2023) completes training of their 3-stage network in around 10 minutes; TC4D (Bahmani et al., 2024)demands approximately 1 hour for the first stage over 10000 epochs, 3 hours for the second stage over 20000 epochs, and roughly 30 hours for the third stage over 30000 epochs.

E 2D HUMAN-OBJECT INTERACTION IMAGE GENERATION

Because of the limited availability of human-object interaction images within the 2D dataset utilized for training diffusion models, existing models encounter challenges in accurately capturing the spatial dynamics and contact between humans and objects. This limitation is evident in Figure 7, where we noticed that during the process of 2D image generation, the diffusion model would struggle to create such images. This inadequacy significantly hampers the ability of diffusion models to generate realistic 3D human-object interactions.

Figure 7: **Example generation of human-object interaction images.** Images generated by pose-conditioned ControlNet Zhang & Agrawala (2023)

F DIRECT RIGGING OF 3D OBJECT AND HUMAN MODELS

We conducted experiments by directly positioning the 3D objects in a reasonable position relative to the humans. As shown in Fig. 8, without further adjustments such as rescaling or rotating, the relationships between humans and objects are not accurately depicted. Penetration issues will also exist in some examples. Even with manual adjustments, such as rescaling and rotating the 3D objects, significant human effort is required, and the interactions between humans and objects still lack accuracy. For instance, Fig. 8 illustrates that humans frequently appear with open hands, which fails to convincingly "hold" the objects and significantly undermines the user experience.

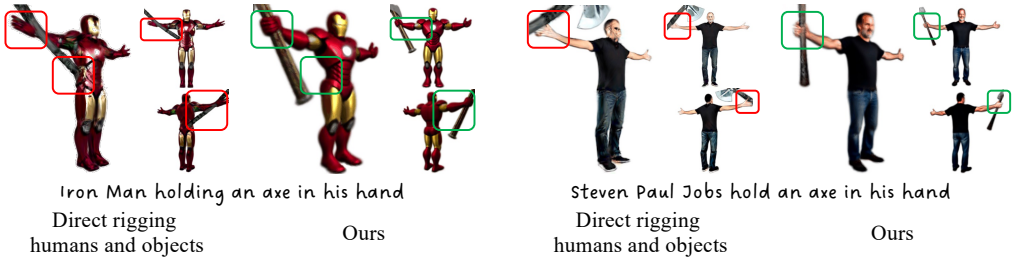

Figure 8: **Evaluation by directly rigging humans and objects**

G ANALYSIS BY DETERMINING THE ANIMATION OF OBJECT BY ONLY THE CONTACT PART

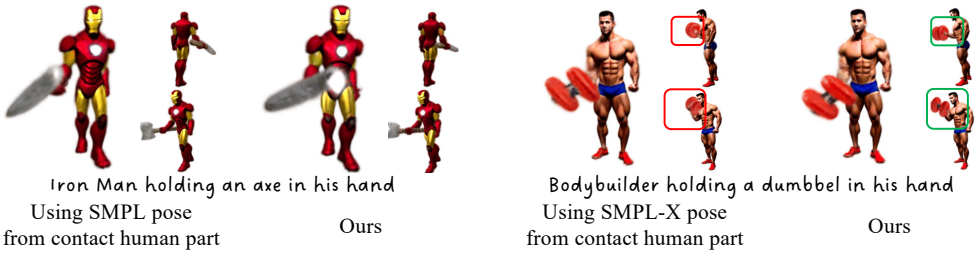

Figure 9: **Evaluation by using SMPL-X pose from contact human part**

We conducted experiments using the contact part of the human body to determine the object's motion. The results are shown in Fig. 9. We found that this approach works well when the object is positioned far from the body, but it can encounter penetration issues when the object is close to the body (see "Bodybuilder holding a dumbbel in his hand"). We will incorporate this discussion into the updated paper.

H COMPARISONS WITH AVATARCRAFT, DREAMWALTZ AND DREAMAVATAR

In Fig. 10, we provide qualitative comparisons with AvatarCraft, DreamWaltz, and DreamAvatar. We observed that AvatarCraft and DreamAvatar are highly constrained by the SMPL prior model, making it difficult for them to create human models with effective object interactions. While DreamWaltz can generate some object interactions, these interactions are often inaccurate. Additionally, DreamWaltz has trouble maintaining proper interactions throughout the animation, as presented in Fig. 11.

Figure 10: **Qualitative comparisons with DreamWaltz, AvatarCraft, and DreamAvatar**

Figure 11: **Evaluation on DreamWaltz's animated results**

I SOCIETAL IMPACT.

The progress in 4D avatar generation with object interactions holds promise for numerous AR/VR applications, yet also raises concerns regarding potential misuse, such as creating misleading or nonexistent human-object pairings. We advocate for responsible research and deployment, promoting openness and transparency in practices to mitigate any potential negative consequences.

J MORE COMPARISONS ON 3D GENERATION

We provide more qualitative comparisons with HumanGaussian (Liu et al., 2023d), GraphDreamer (Gao et al., 2023), and "Ours (`Var-A`)' in Fig. 12. These results serve to reinforce the claims made in Sec. 4 of the main paper, providing further evidence of the superior performance of AvatarGO in compositing 3D human and object models.

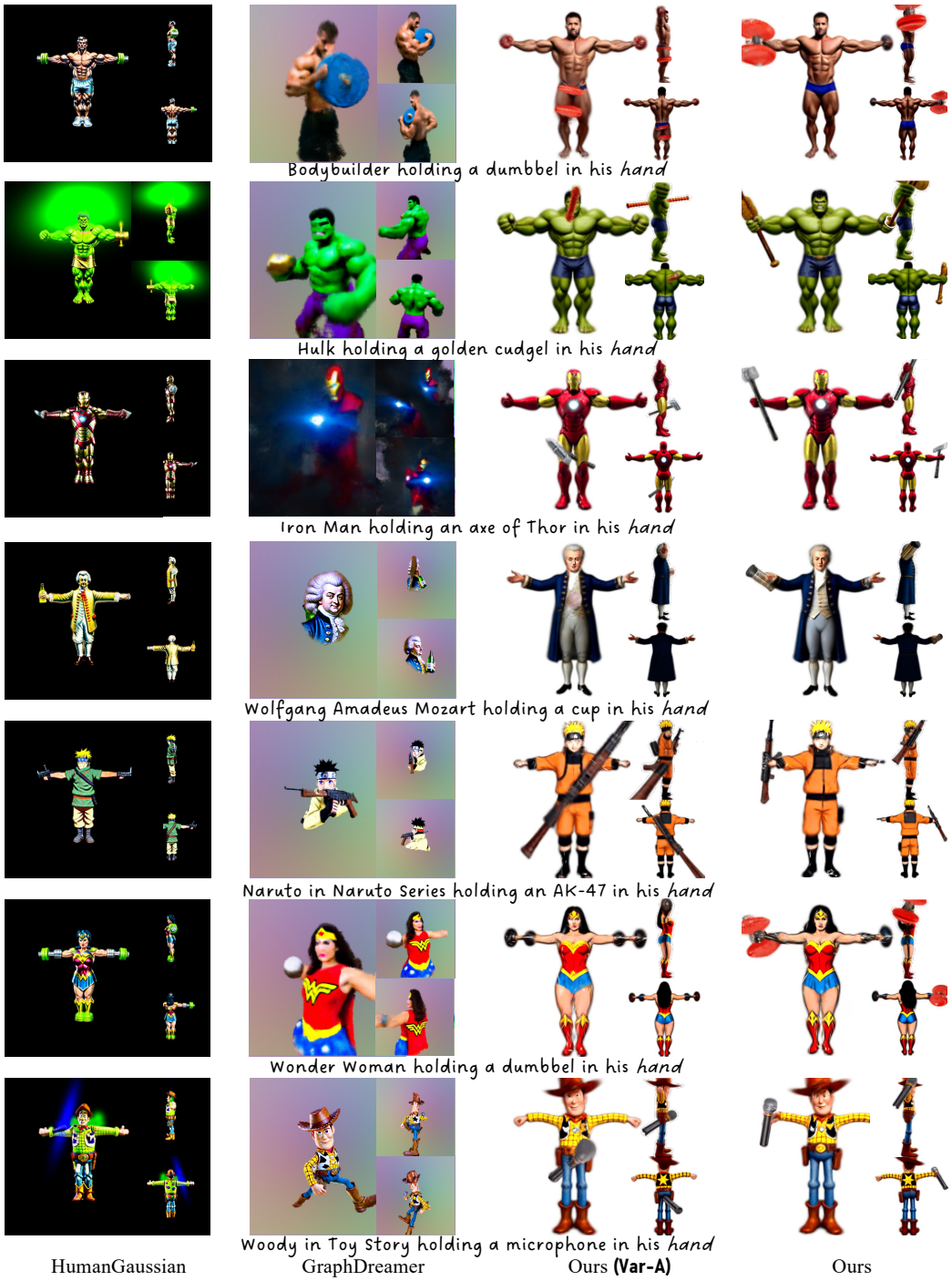

Figure 12: **Comparisons on 3D compositional generations.**

K MORE COMPARISONS ON 4D ANIMATION

We further provide more qualitative comparisons of 4D animation with DreamGaussian4D (Ren et al., 2023), HumanGaussian (Liu et al., 2023d), and "Ours (`Var-B`)'. The results can be found in Fig. 13. These comparisons further demonstrate the superiority of AvatarGO in maintaining the spatial correlation during animations and in addressing the penetration issues.

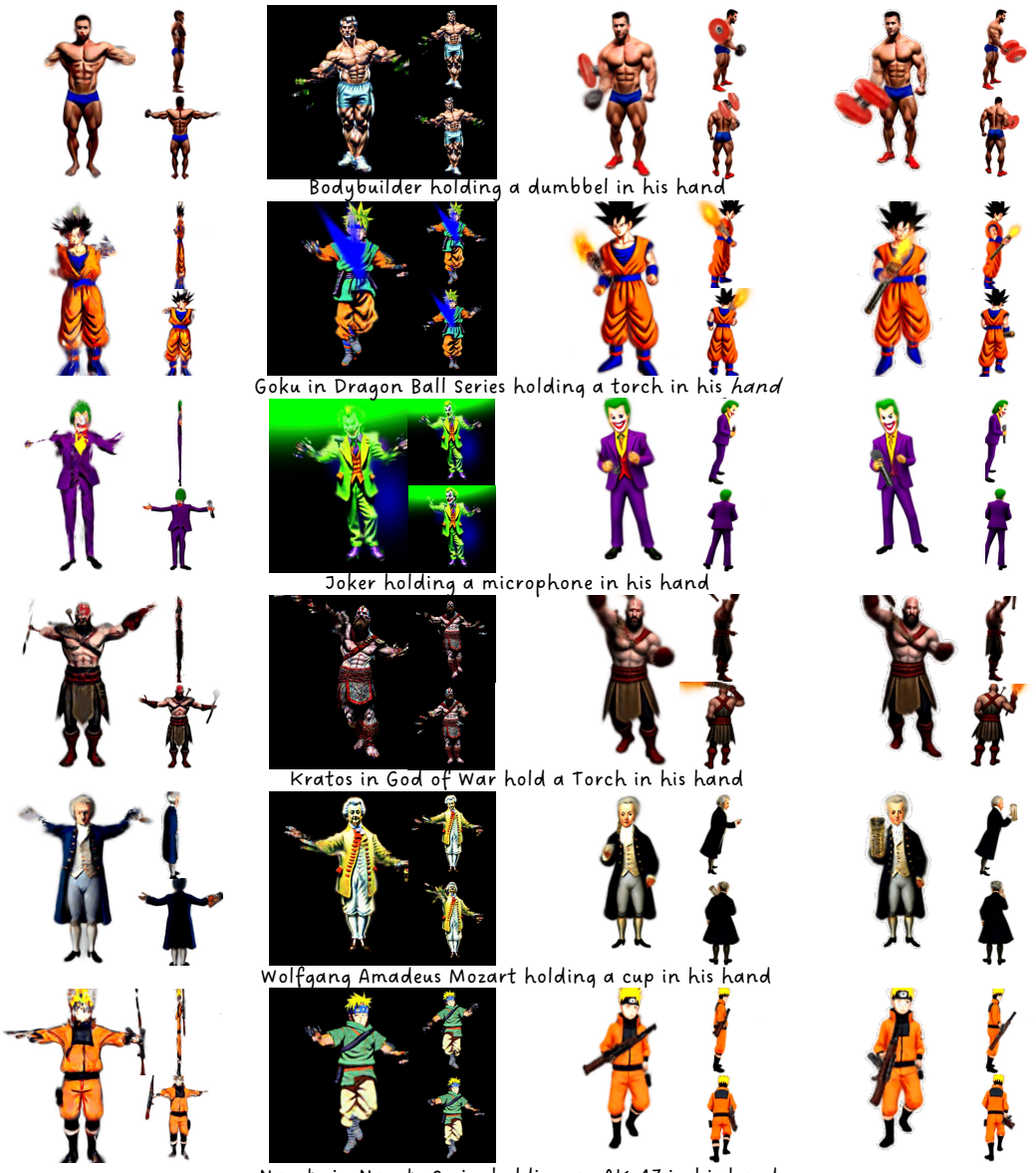

Figure 13: **Comparisons on 4D animation.**